Dielectric, calorimetric and elastic anomalies associated with the first order $I4/mcm \leftrightarrow Pbcm$ phase transition in (Ca, Sr)TiO_3 perovskites

2009 J. Phys.: Condens. Matter 21 295903

(http://iopscience.iop.org/0953-8984/21/29/295903)

J. Phys.: Condens. Matter **21** (2009) 295903 (15pp) doi:10.1088/0953-8984/21/29/295903

Dielectric, calorimetric and elastic anomalies associated with the first order $I4/mcm \leftrightarrow Pbcm$ phase transition in (Ca, Sr)TiO_3 perovskites

J Manchado[1], F J Romero[1], M C Gallardo[1], J del Cerro[1], T W Darling[2], P A Taylor[3], A Buckley[3] and M A Carpenter[3]

[1] Departamento de Física de la Materia Condensada, Instituto Mixto de Ciencia de Materiales CSIC—Universidad de Sevilla, Apartado 1065, 41080 Sevilla, Spain
[2] Department of Physics, University of Nevada, Reno, NV 89577, USA
[3] Department of Earth Sciences, University of Cambridge, Downing Street, Cambridge CB2 3EQ, UK

E-mail: jmanchado@us.es

Received 6 March 2009, in final form 22 May 2009
Published 3 July 2009
Online at stacks.iop.org/JPhysCM/21/295903

Abstract

Conduction calorimetry has been used to determine with high precision the latent heat and variation in heat capacity which accompany the first order $I4/mcm \leftrightarrow Pbcm$ phase transition in perovskites with compositions $(Ca_{1-x}Sr_x)TiO_3$, $x = 0.65, 0.68, 0.74$ (CST65, CST68, CST74). In CST65 (CST68), the latent heat is dissipated/absorbed over a temperature interval of ~11 K (~6 K), which is centred on ~292 K (~258 K) during cooling and ~302 K (~270 K) during heating. The magnitude of the latent heat diminishes with increasing $SrTiO_3$ content and was not detected in CST74. Integration of the latent heat and excess heat capacity yields small excess entropies, which are consistent with the structural changes being displacive rather than order–disorder in origin. Resonant ultrasound spectroscopy measurements on the same CST65 sample as used for dielectric and calorimetric measurements through the same temperature intervals have allowed quantitative correlations to be made with the bulk modulus, shear modulus and acoustic dissipation parameter, Q^{-1}. The dielectric anomaly and changes in Q^{-1} can be understood as being linear combinations of the properties of the separate $I4/mcm$ and $Pbcm$ phases in proportion to their volume fractions across the two-phase field. A change of only ~0.5–1 GPa has been detected in the bulk modulus but the shear modulus softens by ~5–8 GPa as the transition interval is approached from above and below. This shear mode softening presumably reflects clustering and/or phonon softening in both the $I4/mcm$ and $Pbcm$ structures. This pattern of structure–property relations could be typical of first order transitions in perovskites where there is no group/subgroup relationship between the high and low symmetry phases.

1. Introduction

Perovskites from the $CaTiO_3$–$SrTiO_3$ (CST) solid solution have attracted considerable attention due to their unusual diversity of phase transitions involving both octahedral tilting and ferroelectric/antiferroelectric/relaxor type atomic displacements (Mitsui and Westphal 1961, Bednorz and Müller 1984, Bianchi *et al* 1994a, 1994b, 1995, Bianchi 1996, Kleemann *et al* 1995, 1997, Hirata *et al* 1996, Lemanov 1997, Ball *et al* 1998, Hayward and Salje 1999, Ranjan and Pandey 1999, 2001a, 2001b, Ranjan *et al* 1999, 2000, 2001, Qin *et al* 2000, 2002, Carpenter *et al* 2001, 2006b, 2007a, 2007b, Mishra *et al* 2001, 2002, 2005, 2006a, 2006b, Ouillon *et al* 2002, Yamanaka *et al* 2002, Gallardo *et al* 2003, Harrison

et al 2003, Ranson *et al* 2005, Howard *et al* 2001, 2005, 2008, Daniels *et al* 2006, Woodward *et al* 2006, Carpenter 2007a, 2007b, Anwar and Lalla 2007, 2008, Hui *et al* 2007, Walsh *et al* 2008), their potential as stable hosts for immobilizing radioactive waste elements (Ringwood *et al* 1988) and their structural analogies with silicate perovskites which exist in the Earth's mantle (Qin *et al* 2000, 2002, Carpenter *et al* 2001, 2007a, Harrison *et al* 2003, Carpenter 2007a, 2007b, Walsh *et al* 2008). The structure of each phase and the sequence of phase transitions across the solid solution have been controversial, though an attempt to correlate all the known transition behaviour has recently been assembled as a phase diagram (Carpenter *et al* 2006b).

At high temperatures, the stable CST phase is cubic ($Pm\bar{3}m$). At lower temperatures, a tetragonal phase ($I4/mcm$) develops as a consequence of an octahedral tilting transition associated with the R point of the Brillouin zone. At Ca-rich compositions an additional first order phase transition to an orthorhombic $Pnma$ structure occurs. A structure with $Pbcm$ symmetry develops in place of this at compositions which are more Sr-rich than $\sim Ca_{0.4}Sr_{0.6}TiO_3$, while $SrTiO_3$ doped with Ca develops a ferroelectric structure below ~35 K. The Sr-rich half of the phase diagram of Carpenter *et al* (2006b) is reproduced in figure 1 to show the relevant structural relationships. All these structure types have differences in their physical and thermodynamic properties but it has been difficult to determine robust structure–property relationships for them because of the discrepancies between reported structures and transition temperatures in many studies. At least some of the variations must be due to different sample preparation methods, which presumably have resulted in different grain sizes, stoichiometry and defect contents, so the present study has been aimed at generating a coherent set of thermodynamic, elasticity and dielectric data from a single sample of $Ca_{0.35}Sr_{0.65}TiO_3$ (CST65). The specific focus is on how properties evolve in detail through the first order transition at which the $Pbcm$ structure appears. Two other compositions have also been investigated to allow correlations between trends of calorimetric properties with trends in dielectric properties reported in the literature.

Thermal properties almost invariably provide fundamental insights into the energetic aspects of a phase transition and can also shed light on transition mechanisms. The presence of latent heat confirms discontinuous character for a transition, for example, and specific heat integrates the contributions of different order parameter components. Although there are measurements of specific heat and latent heat for the $I4/mcm \leftrightarrow Pnma$ transition in CST0 (Guyot *et al* 1993) and CST50 (Qin *et al* 2000), no data appear to be available for the proposed $I4/mcm \leftrightarrow Pbcm$ phase boundary. The Seville group has developed an original technique based on conduction calorimetry, which provides absolute values of the specific heat and allows latent heats to be determined separately to exceptionally high precision (del Cerro *et al* 2000, 2003). The method has been successfully applied to a variety of materials (Gallardo *et al* 2000, Martín-Olalla *et al* 2000, Romero *et al* 2001, 2004a, 2004b, Delgado-Sanchez *et al* 2005, Romero *et al* 2006, 2007).

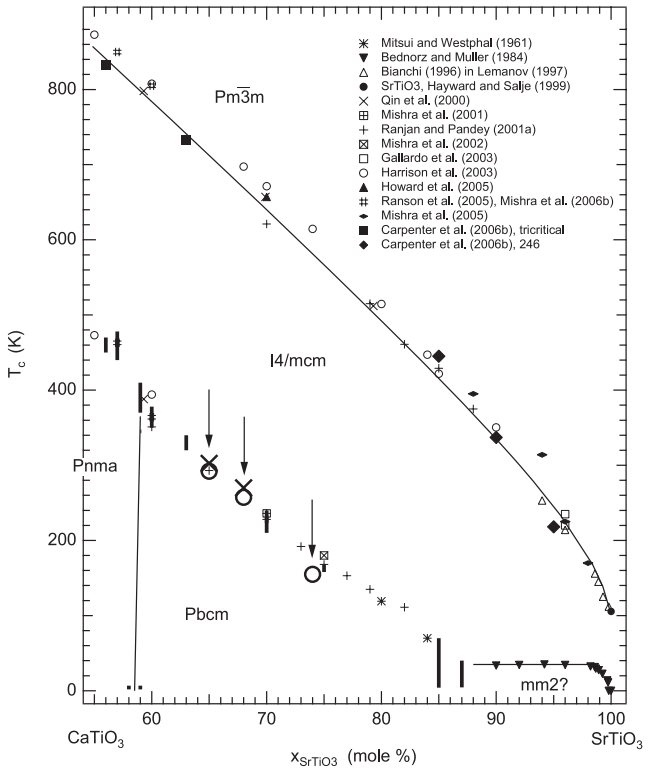

Figure 1. The $SrTiO_3$-rich end of the $CaTiO_3$–$SrTiO_3$ phase diagram, reproduced after Carpenter *et al* (2006b). Vertical solid bars are estimates of the temperature intervals within which orthorhombic and tetragonal structures coexist at a variety of different compositions, based on diffraction data of Ranjan and Pandey (2001a), Carpenter *et al* (2006b) and Mishra *et al* (2006b). Arrows highlight compositions investigated in the present study: large circles and large crosses signify the temperatures at which the specific heat reached a maximum during cooling and heating, respectively. The circle for CST74 represents a transition temperature estimated from the heat capacity anomaly observed during cooling.

Calorimetric and dielectric results for CST65, CST68 and CST74 are reported here along with elasticity and anelasticity data collected from the CST65 sample by resonant ultrasound spectroscopy in Cambridge. It is worth pointing out that first order transitions between structures which do not have a group–subgroup relationship are common among perovskites and that the results given below might have a significance which goes beyond the specific case of CST.

2. Experimental details

2.1. Sample preparation and characterization

Samples of $Ca_{0.35}Sr_{0.65}TiO_3$ (CST65), $Ca_{0.32}Sr_{0.68}TiO_3$ (CST68) and $Ca_{0.26}Sr_{0.74}TiO_3$ (CST74) have been investigated. The CST65 powder used to prepare a polycrystalline pellet for calorimetric, dielectric and RUS measurements was the same as that used by Carpenter *et al* (2007a, 2007b). It had been synthesized using the procedure developed by Ball *et al* (1998). Ca and Sr nitrates were dissolved in water and mixed with Ti-isopropoxide, and the resulting gel-like material dried, ground and calcined. The product was ground in an agate ball mill and

subjected to three further firing and grinding cycles. The first firing was for 36 h at 1350 °C, the second for 12 h at 1600 °C and the third for 36 h at 1600 °C. The sample was finally disaggregated in the ball mill at a slower speed than had been used for intermediate grinding stages (300 rpm instead of 600 rpm). The resulting pale cream powder gave sharp peaks due to perovskite in a standard room temperature x-ray powder diffraction pattern. One barely detectable peak corresponding to a d-spacing of ∼3.23 A was observed, indicating the presence of rutile as an impurity phase. The Ca:Sr ratio of a sintered fragment of the sample was checked on a Cameca SX-100 electron microprobe but an independent determination of the oxygen content has not been obtained. Following the recipe of Walsh *et al* (2008), 2 g of the CST65 powder was pressed into a pellet under vacuum in a steel die for ∼5 min at ∼20 MPa. The pellet was fired in air for 48 h at 1600 °C, with ramping up from room temperature and back down again at a rate of 10 °C min^{-1}. The hard ceramic product was finally ground down to a disc with closely parallel faces, 10.0 mm in diameter, 3.650 mm thick and weighing 1.2723 g. After this disc had been used for dielectric and calorimetric measurements, a rectangular parallelepiped was cut from it using a fine annular saw lubricated with paraffin. The parallelepiped had dimensions 3.666 mm × 2.707 mm × 3.669 mm and mass 0.1612 g, and was used for RUS measurements. Using lattice parameter data of Ball *et al* (1998), and a measured density based on the dimensions and mass of the parallelepiped (4.427 g cm^{-3}), the density of the ceramic was found to be 93.4% of the theoretical density. The remaining 6.6% is assumed to be due to porosity. Observations in a petrographic microscopic of thin sections of other CST ceramic samples produced using essentially the same recipe suggest that the grain size was probably ∼25 μm (Walsh *et al* 2008). It should be emphasized that, apart from the different dimensions, the same sample was used for dielectric, calorimetric and RUS measurements.

CST68 and CST74 were synthesized at the University of Bayreuth (Qin *et al* 2000) by first drying the reagents $CaCO_3$ (Chempur, 99.9%) and $SrCO_3$ (Aldrich, 99.999%) at 500 °C, and TiO_2 (Aldrich, 99.9%) at 1000 °C for 3 h. Stoichiometric mixtures of these were heated to 1300 °C at a rate of 20 °C h^{-1} and kept at that temperature for 4 h. After grinding in an agate mortar, the samples were fired in air at 1600 °C for 48 h with periodic regrinding, and finally rapidly cooled. Analysis by microprobe showed them to be close to the nominal compositions and homogeneous at the 1% level. The powders were pressed and sintered at 1600 °C for 24 h to produce pellets with closely parallel faces. The resulting sample of CST68 was a disc 9.4 mm in diameter, 3.850 mm thick and weighing 1.1478 g. The corresponding sample of CST74 was a disc 9.3 mm in diameter, 4.870 mm thick and weighing 1.4933 g.

2.2. Calorimetric measurements

Measurements of heat flux and specific heat were performed using a high resolution conduction calorimeter, which has been described in detail elsewhere (Gallardo *et al* 1995). In this instrument, the sample is pressed between two identical heat fluxmeters, which are made from 50 chromel-constantan thermocouples connected in series, with the wires placed in parallel lines (Jiménez *et al* 1984). Two electrical resistance heaters are placed between each face of the sample and the fluxmeters. These can dissipate a uniform heat power on the sample faces.

Specific heat is measured using the method previously described (del Cerro 1988). The same constant power is dissipated in both heaters (dissipation branch) for 12 min to reach a steady state characterized by a constant temperature difference between the sample and the calorimeter block (less than 0.05 K). Power is then cut off until a new steady state is reached (relaxation branch). The power is then switched on again and the sequence is continuously repeated while the temperature of the assembly is changed at a constant, low rate. In this way, a long-periodic series of square thermal pulses is superimposed on a heating or cooling ramp of 0.1 K h^{-1}. Integration of the emf given by the fluxmeters between every pair of steady state distributions allows the thermal capacity of the sample to be determined. It should be pointed out that two specific heat data are obtained in each cycle, one from the dissipation branch (c_d) and another from the relaxation branch (c_r).

The equipment works also like a very sensitive differential thermal analysis (DTA) device. A DTA trace is continuously measured in a second run without dissipation in the sample, using the same temperature scanning rate as applied during measurement of the specific heat. The emf given by the fluxmeters is proportional to the heat flux, ϕ_D, the integral of which, in turn, is proportional to the total enthalpy change of the sample.

The heat flux can have two contributions, one due to the latent heat and another due to the variation of specific heat with temperature of the sample. In an idealized first order transition, the latent heat would appear as a spike in the heat flux, which would be trivial to separate from the specific heat. In reality, the transition occurs over a range of temperatures and the latent heat is smeared out, so overlapping with the specific heat contribution. This difficulty can be overcome (del Cerro *et al* 2000). From the specific heat data obtained in the first run, the heat flux which would correspond exclusively to the thermal capacity behaviour around the transition temperature, ϕ_c, is calculated. If the transition is continuous, ϕ_D and ϕ_c coincide over the entire temperature range. When a first order phase transition takes place, ϕ_D and ϕ_c do not coincide in the temperature range, T_1–T_2, where the latent heat is present. This interval corresponds to the two-phase field for the transition. The value of the latent heat is obtained by integration between T_1 and T_2 of ϕ_D/v, where v is the temperature scanning rate, with respect to the appropriate baseline. The sensitivity of this method is estimated to be better than 5 mJ, even when the specific heat shows a strong anomaly at the transition.

2.3. Dielectric measurements

The dielectric constant was measured using a capacitance bridge ESI-SP 5400 at a frequency of 1 kHz in a cell different to that used to perform thermal properties measurements. The

temperature stability of this device is estimated to be ∼0.01 K. To perform the dielectric measurements, the plane faces of the samples were coated with silver paint.

2.4. Resonant ultrasound spectroscopy (RUS) measurements

The equipment used to collect RUS spectra at low temperatures has been described in detail by McKnight *et al* (2007). Spectra were collected from the CST65 parallelepiped in the frequency range 0.35 or 0.4 to 1.2 MHz, with 50 000 data points per spectrum. Two separate data sets were collected. For the first, temperature was cycled in 1 K steps from 307.8 to 262.7, from 263.6 to 306.6 K, from 312.5 to 278.4 and finally from 279.2 to 313.0. At each point and before data collection a delay of 15 min was used to allow complete thermal equilibration. In the second experiment, the parallelepiped was cooled to 10.8 K in 30 K steps and then heated from 10.8 to 268.3 K in ∼10 K steps, followed by 268.3 to 312.5 K in ∼5 K steps and 312.5 to 278.8 K in 5 K steps, again with a thermal equilibration period of 15 min before data collection at each temperature. The thermocouple next to the sample gave an accurate reading at room temperature and, from a separate investigation, also gave readings which were within 1 K of the expected transition temperature of 106 K in a sample of $SrTiO_3$ (McKnight *et al* 2009b). Following the collection of low temperature data, the parallelepiped was transferred to the high temperature instrument described by McKnight *et al* (2008). Spectra were collected in the same frequency range as in the low temperature instrument at 5 K intervals during heating from ∼300 to ∼480 K and then back to ∼300 K. An equilibration time of 15 min was again used to allow thermal equilibration at each set point. McKnight *et al* (2009a) checked readings from the thermocouple sited close to the sample in the high temperature instrument against the known phase transition temperatures of quartz, $LaAlO_3$ and CST70 and their calibration has been applied to the temperatures given for data in the figures below. The estimated accuracy of these temperatures is ±1 K.

Raw spectra were transferred to the software package Igor Pro (wavemetrics) for analysis. Room temperature values of the bulk (K) and shear (G) moduli were determined using DRS software as described by Migliori and Sarrao (1997). The fitting process yielded $K = 144.6 \pm 0.8$, $G = 76.09 \pm 0.05$ GPa from measured frequencies of 36 resonance peaks, with an RMS error of 0.21%. Correction for the influence of 6.6% porosity using the expressions of Ledbetter *et al* (1994) then gave $K = 169.9$ and $G = 86.4$ GPa for a fully dense ceramic, in line with ultrasonic and equation of state measurements for the same composition (Carpenter *et al* 2007a, 2007b) and in agreement with data for other compositions given by Walsh *et al* (2008). Values of K and G were also determined from the frequencies of 22–25 peaks in spectra from the sequence of heating and cooling through the transition in 1 K steps. These had RMS errors of 0.24–0.30% and slightly greater uncertainties than obtained for the individual values at room temperature. The frequency, f, and line width at half height, Δf, of a resonance peak near 0.95 MHz in all the low temperature spectra were determined by fitting with an asymmetric Lorentzian function (McKnight *et al* 2007, 2008, 2009a, 2009b). This peak was chosen for analysis because of its intensity and lack of overlap with adjacent peaks. The mechanical quality factor, Q, was calculated as $Q = f/\Delta f$; Q^{-1} is a measure of acoustic dissipation in the sample. Rather than refine every data set from the second low temperature series, values of G were obtained by a simple calibration. Each resonance peak in an RUS spectrum is due to a particular distortion mode and the square of its frequency scales linearly with the effective elastic constant for that mode (Migliori and Sarrao 1997). For an isotropic ceramic material with the elastic constants of CST perovskites the frequency of most resonances is determined largely by the shear modulus (G), with generally only small contributions from the bulk modulus (K). For the peak near 0.95 MHz the DRS software indicated control by ∼86% shear and ∼14% bulk modulus. A calibration of f^2 for this peak using the fitted values of G yielded two linear relationships, one for above the transition point and one for below, and these were used to estimate values of G for the remaining low temperature data.

The high temperature RUS instrument gives weaker resonance spectra than the low T instrument because the sample is separated from the transducers by alumina rods rather than sitting directly on them. As a consequence the peak near 0.95 MHz was too weak to yield reliable linewidths. It was possible to measure peak frequencies up to ∼430 K, however, and these were used to calculate values of G. The peak at ∼0.45 MHz, on the other hand, was sufficiently strong to yield both peak positions and widths using the fitting procedure described above, allowing values of Q to be obtained up to temperatures of ∼480 K.

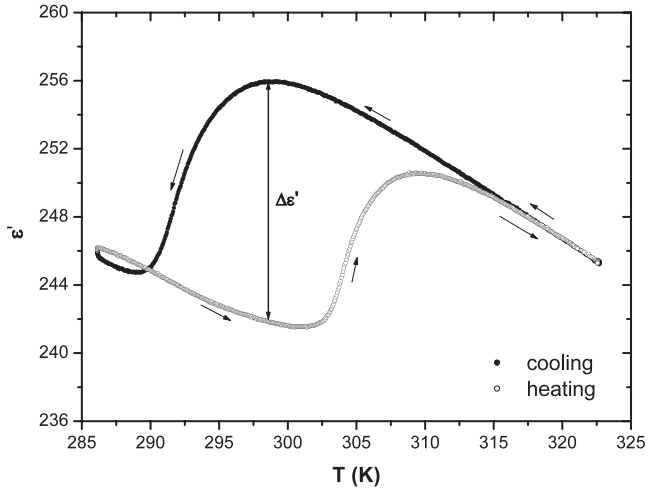

Figure 2. Dielectric permittivity versus temperature for CST65 measured during cooling and heating. $\Delta\varepsilon'$ is the difference in values of ε' between the high temperature ($I4/mcm$) and low temperature ($Pbcm$) phases in the vicinity of the $I4/mcm \leftrightarrow Pbcm$ transition.

3. Results

3.1. Dielectric permittivity

Figure 2 shows a typical curve of the dielectric permittivity ε' for CST65 at 1 kHz obtained on cooling and heating the sample

at 0.5 K h^{-1}. A thermal hysteresis of about 10 K is observed in the temperature of the maximum of the anomaly which suggests a discontinuous character for the phase transition. In other samples of $(Ca_{1-x}Sr_x)TiO_3$, Ranjan *et al* (2000) and Ranjan and Pandey (2001a) have fit a Curie–Weiss law to the high temperature data, yielding negative values of the Curie temperature, which has been associated with antiferroelectric character of the phase transition. If a similar fit is made to the high temperature data obtained in this study, a negative Curie temperature is obtained ($T_c \sim -154$ K). Similar results were obtained for CST68 and CST74, and these agree closely in form with data from the literature, confirming comparability between the samples (composition, structural state, chemical homogeneity, etc) prepared for this study and samples used by other workers.

3.2. Thermal properties

The temperature dependences of the specific heat c_p for CST65 and CST68 are shown in figures 3(a) and (b), respectively. A smeared anomaly was found in heating and cooling runs but with a significant thermal hysteresis of about 11 K between the temperatures of the maximum of the anomalies. The specific heat obtained for CST74 in cooling runs is shown in figure 3(c). This sample gave a broad anomaly during cooling but no anomaly was detected during heating, probably due to smearing of the peak.

The first point to note is that the transition temperatures are in agreement with the phase diagram reported previously. The temperatures of the specific heat maximum for the different samples have been added to figure 1 and, in the cases of CST65 and CST68, fall within the range of the proposed $I4/mcm$–$Pbcm$ phase boundary obtained in previous studies. The maximum for CST74 falls a few degrees below other data (figure 1).

In order to analyse the excess specific heat, Δc, a baseline has been calculated for CST65 which has the curvature of the measured specific heat for CST68, since the compositions are similar and the results for CST68 do not include any anomaly in the transition interval of CST65. A similar procedure was used for CST68, using the specific heat for CST74 as the reference curve. Finally, the baseline for CST74 was obtained as a second order polynomial fit to data well above and below the specific heat anomaly. The specific heat excess increases in the phase transition interval, reaches a practically constant value at lower temperatures and amounts to less than 0.8% of the total. Maximum values of Δc are $\sim$0.8 J mol^{-1} K^{-1} for CST65, $\sim$0.6 J mol^{-1} K^{-1} for CST68 and $\sim$0.5 J mol^{-1} K^{-1} for CST74. A significant thermal hysteresis between heating and cooling experiments was obtained for CST65 and CST68, which is a characteristic feature of a first order transition.

In order to analyse in depth the mechanism and nature of the phase transition, DTA traces were obtained in a second run for each sample, changing the temperature at a constant rate similar to that used in specific heat measurements. It should be noted that the temperature scanning rate used was two orders of magnitude lower than the minimum value achieved in conventional DTA devices. DTA traces obtained for CST65 in heating and cooling runs are shown in figures 4(a) and (b), and an anomaly spread across $\sim$11 K is evident in both cases. Following a previously described procedure (del Cerro *et al*

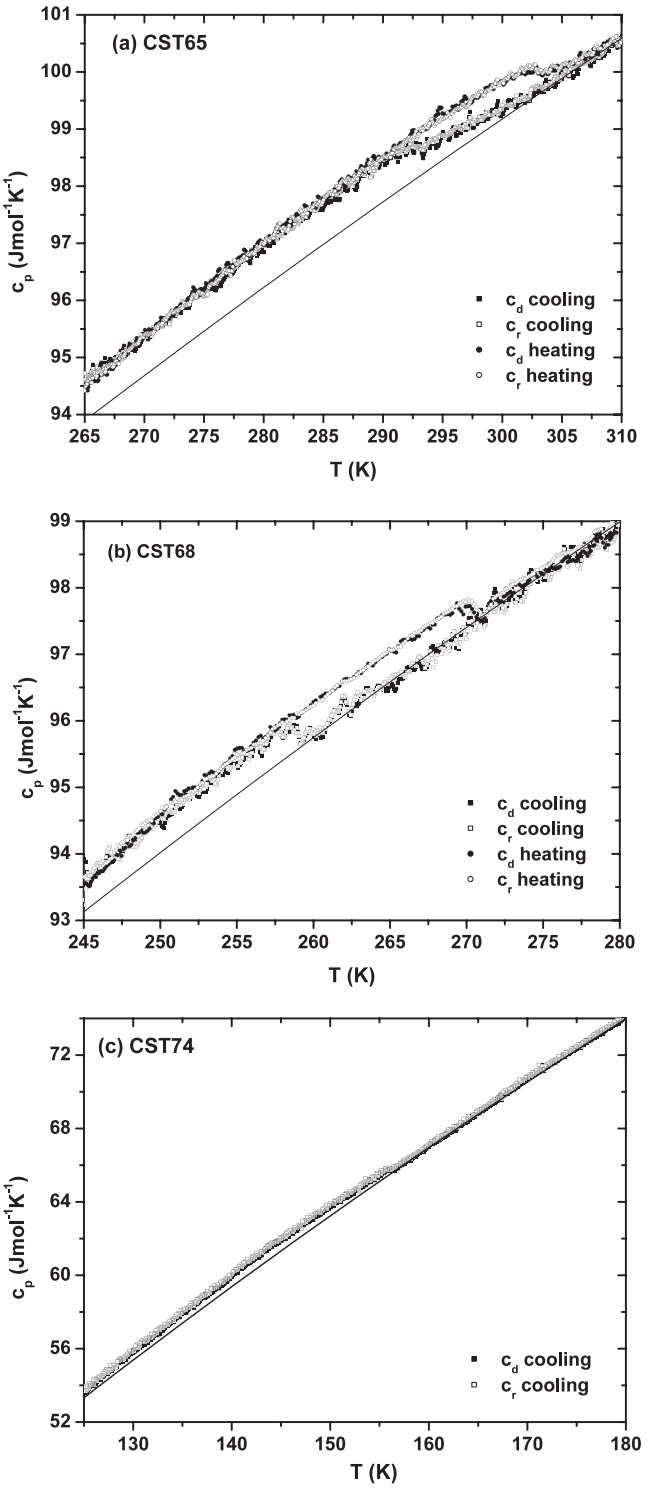

Figure 3. Temperature dependence of the specific heat for CST65 (a), CST68 (b) and CST74 (c). Data for the dissipation branch (filled squares on cooling and filled circles on heating) and for the relaxation branch (open squares on cooling and open circles on heating) have been included. The baseline used to determine the excess specific heat excess is shown as a solid line in each case.

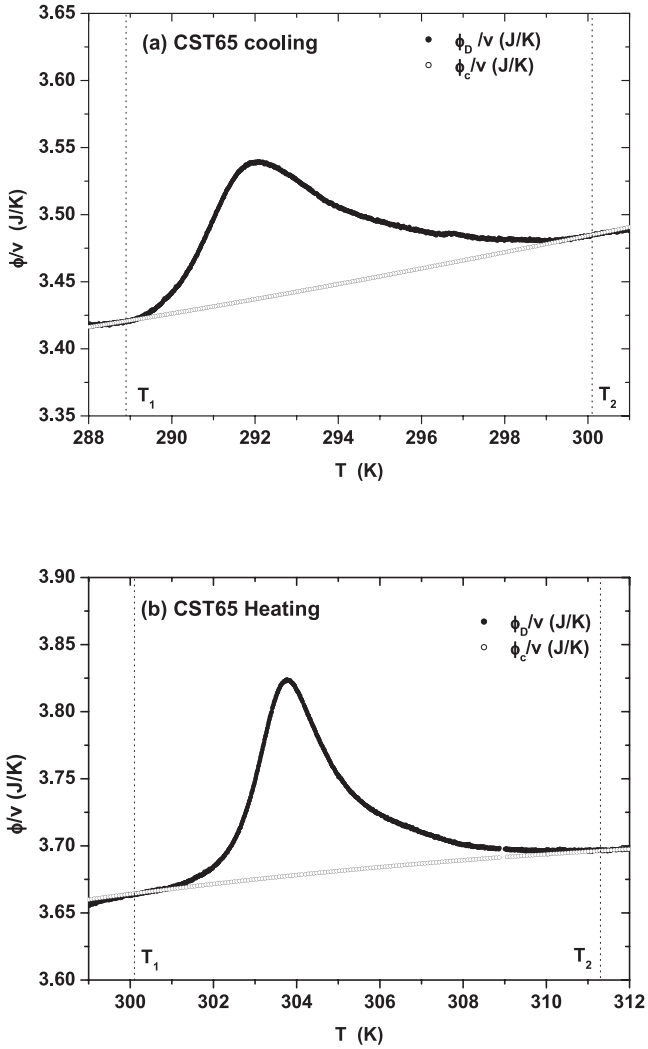

Figure 4. DTA trace ϕ_D/v (filled circles) for CST65 for cooling (a) and heating (b). The contribution to the DTA trace due to the temperature dependence of the specific heat, ϕ_c/v, is indicated by open circles.

2000), the contribution to the heat flux due to the temperature dependence of the specific heat (ϕ_c/v) has been calculated and is represented by open circles in figure 4. The anomaly in the experimental DTA trace (ϕ_D/v) is clearly larger than the calculated contribution from the specific heat in the interval T_1 to T_2. This result indicates that a first order phase transition has taken place and that the latent heat is developed between T_1 and T_2, which corresponds to the two-phase field. Similar results have been found in the heat flux analysis for CST68. Values of T_1 and T_2 and the extent of the two-phase field $d = T_2 - T_1$ are listed in table 1.

Values of the latent heat, L, for the transition have been calculated by integration of ϕ_D/v with respect to ϕ_c/v between T_1 and T_2, and are also given in table 1. Note that the latent heat measured during cooling is higher than during heating for each of CST65 and CST68. The excess specific heat during heating is larger than during cooling and contributes more to the enthalpy. Thus, in order to maintain the enthalpy balance, L must be smaller during heating than during cooling. A

Table 1. Latent heat, L, and limiting temperatures, T_1 and T_2, for the two-phase interval detected during heating and cooling of CST65 and CST68 ($d = T_2 - T_1$).

	L (J mol^{-1})	T_1 (K)	T_2 (K)	d (K)
CST65 cooling	55.36	289.2	299.7	10.5
CST65 heating	49.76	300.5	311.5	11.0
CST68 cooling	30.19	256.6	262.2	5.6
CST68 heating	26.50	269.5	276.1	6.6

significant reduction of latent heat is found when the amount of Sr is increased and none was detected in the case of CST74. If the transition is first order, in accordance with symmetry arguments, L for the latter sample is either very small or is spread over a wide temperature interval so that it is not detected.

In high resolution calorimetric investigations of first order transitions, it is expected that c_d and c_r will be very different within the temperature interval where latent heat is released or absorbed (del Cerro *et al* 2003). The difference has been found to be significant even in crystals near the tricritical point, where the latent heat is very small ($L = 19.5$ J mol^{-1} for $KMnF_3$, 1.5 J mol^{-1} for $KMn_{0.997}Ca_{0.003}F_3$), but in these cases the transition takes place in a very narrow temperature interval (0.3 K for $KMnF_3$:Ca, 0.1 K for DTGSe). The latent heat dissipated or absorbed during each thermal pulse (0.05 K of amplitude) in the process of measurement of the specific heat is sufficient to disturb the measurement, causing differences between the dissipation and relaxation semiperiods in the specific heat measurement process. In marked contrast, c_d and c_r coincide (figures 3(a) and (b)) over the entire temperature transition interval for CST65 and CST68, in spite of the latent heat. The total latent heat is significantly higher than for the previously described systems, but its release/absorption is spread over a much wider temperature interval such that the amplitude of each thermal pulse during the specific heat measurement (0.05 K) is much smaller than the interval over which the latent heat is produced (around 5–10 K). Because of this spread, the amount of latent heat dissipated or absorbed due to the first order phase transition during each thermal pulse is not enough to affect significantly the specific heat measurement process. The difference between c_d and c_r due to latent heat is then lower than the scatter in the experimental data. This is an important result in that it shows that the transition mechanism involves latent heat being produced gradually through the sample across a wide (5–10 K) transition temperature interval rather than occurring at a discrete transition point.

Energetic characterization of the transition in terms of the excess entropy, ΔS, has been obtained by integration of Δc, $\Delta S_c = \int \frac{\Delta c}{T} \mathrm{d}T$, and L, $\Delta S_L = \int \frac{\phi_D - \phi_c}{vT} \mathrm{d}T$. The variation of ΔS obtained for CST65 is similar in form for heating and cooling (figure 5(a)), with the largest contributions coming from the latent heat and the quasilinear variation below the transition interval being due to the specific heat. Although L is larger for cooling than for heating, the contribution of Δc is sufficient to produce a full entropy balance. Similar results were also obtained for CST68 (figure 5(b)).

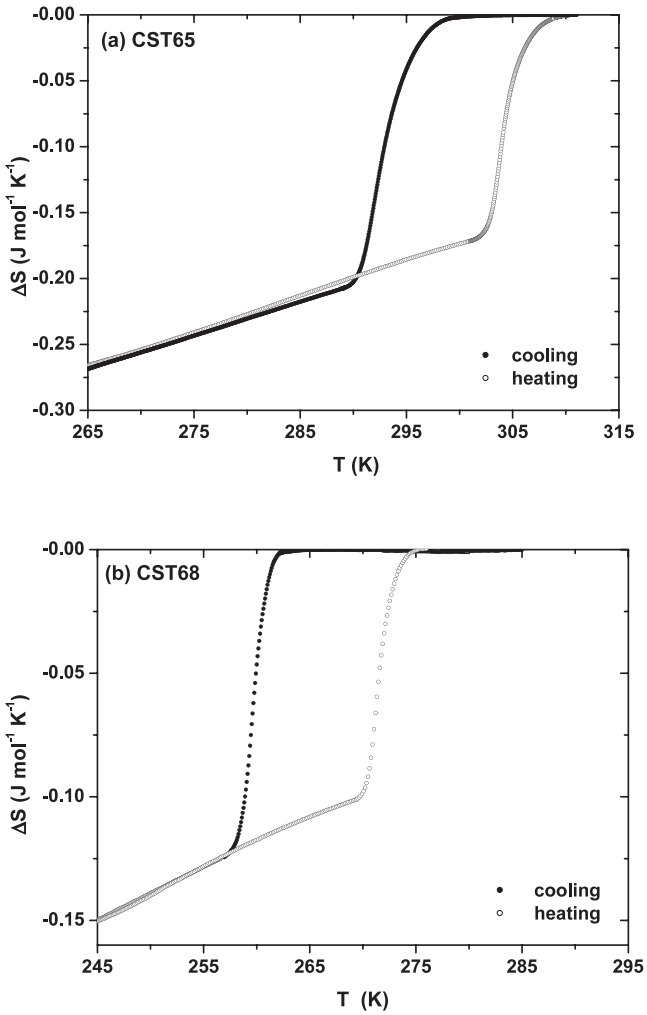

Figure 5. Excess entropy for CST65 (a) and CST68 (b) respect to the high temperature phase, in heating and cooling runs, obtained by integration of the latent heat and excess specific heat.

3.3. Resonant ultrasound spectroscopy

Successive cycles through the $I4/mcm \leftrightarrow Pbcm$ transition interval in the RUS cryostat revealed reproducible and distinct differences between heating and cooling. These are illustrated using segments of spectra obtained during cooling from 312.5 to 278.4 (figure 6(a)) and then heating back to 313.0 K (figure 6(b)). The pattern of evolution of all resonance peaks is the same, with clear breaks in the trend of frequency with temperature. Variations in K, G and Q^{-1} for the ∼0.95 MHz peak in these spectra are given in figure 7. Broken lines have been added to show the temperatures at which minima in peak frequencies occur in the raw spectra (∼291.8 K during cooling and at ∼303.5 K during heating). The trend of G towards these temperatures is linear from below and markedly curved from above (figure 7(a)). The bulk modulus is more or less constant above and below the transition interval and varies by only ∼1 GPa in total (figure 7(a)). This change is less than the absolute uncertainty in the measurements but, given that the spectra were all collected and analysed in the same way, is at least an internally consistent estimate of the slight stiffening that occurs during cooling. The small peak in K near 292 (cooling) and 304 K (heating) also appears to be real. Hysteresis curves for Q^{-1} through the same temperature sequences (figure 7(b)) are similar in form to those for the shear modulus, but differ in showing marked curvature both below and above the temperature at which G reaches a minimum value. The minimum point for G during both heating and cooling is marked by a change in curvature of Q^{-1} such that the change per degree temperature change ($\mathrm{d}Q^{-1}/\mathrm{d}T$) reaches a maximum value (figure 7(c)).

Figure 8 includes data for G and Q^{-1} from spectra collected over wider temperature ranges above and below the transition temperature interval, in addition to the data from figure 7. The primary spectra were collected at slightly faster heating and cooling rates than the spectra in figure 6, but the values of G extracted from them are indistinguishable at temperatures where they overlap. From the perspective of the bulk elastic properties, changes in structural state through the phase transition are both quantitatively reproducible and independent of heating/cooling rate. There is a small hysteresis in peak frequencies associated with heating to ∼480 K and back to room temperature which is probably due to a change in transformation twin configurations if the twin walls become mobile at the highest temperatures. With respect to shear, the high temperature structure is ∼4 GPa softer than the low temperature structure at temperatures well away from the transition interval. Marked softening occurs in both structures as the transition is approached.

Data for Q^{-1} in figure 8(b) are from the 0.95 MHz peak for temperatures between 10 and 313 K, and from the 0.45 MHz peak for temperatures between ∼300 and ∼490 K. In the interval close to room temperature where the two data sets overlap, there is close agreement between values obtained from the two resonance peaks. At high temperatures, increasing scatter is due to the fact that the 0.45 MHz peak became weaker and progressively more influenced by noise in the baseline. Below the transition temperature interval, acoustic dissipation is very low ($Q^{-1} < 0.0005$) and indistinguishable for heating and cooling at different rates. The transition interval corresponds to a step increase from ∼0.0005 for the low temperature structure to ∼0.002 for the high temperature structure. Above ∼350 K, dissipation increases substantially, and by ∼480 K the resonance peaks have all but disappeared. Total attenuation of acoustic resonances ('superattenuation') has been reported for $LaAlO_3$ (Carpenter *et al* 2006a), and is most probably due to local movement of twin walls under low stress. Migliori and Sarrao (1997) noted the loss of resonance peaks below the $Pm\bar{3}m \leftrightarrow I4/mcm$ transition in $SrTiO_3$ and Walsh *et al* (2008) found that resonance peaks were totally attenuated in the stability field of the $I4/mcm$ structure of $Ca_{0.5}Sr_{0.5}TiO_3$. High attenuation is also a characteristic feature of the $Imma$ and $I4/mcm$ phases of Sr(Zr, Ti)O_3 (McKnight *et al* 2009a, 2009b). The pattern of dissipation through the transition interval in CST65, however, is quite different from the usual pattern of elastic and anelastic behaviour at first order transitions in perovskites. A maximum in dissipation characteristically occurs at the same temperature as a minimum in the elastic constants, as seen at the $P4mm \leftrightarrow Amm2 \leftrightarrow R3m$ transitions in $(Ba_{0.8}Sr_{0.2})TiO_3$ (Wang *et al* 2007), for example.

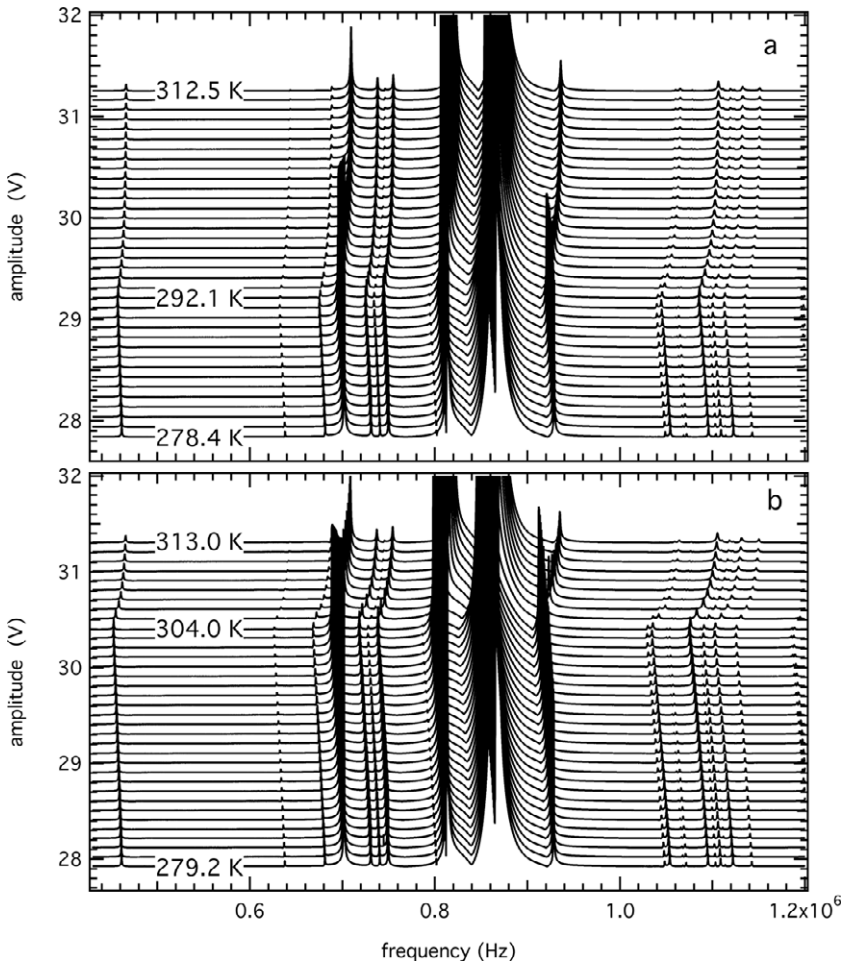

Figure 6. RUS spectra collected at ∼1 K intervals during cooling (a) and heating (b) through the $I4/mcm \leftrightarrow Pbcm$ transition in CST65. The y-axis represents the amplitude of the RUS signal in volts but individual spectra have been offset in proportion to the temperature at which they were collected.

4. Discussion

Discrepancies remain in the literature as to the phase diagram for $SrTiO_3$-rich compositions in the CST system, but published data are sufficient to suggest that the transition in CST65, CST68 and CST74 investigated in the present study is the same as has been examined by others in the same composition range. In particular, the anomalies in dielectric properties shown in figure 2 for CST 65 and observed for CST68 and CST74 have the same form as those reported for different compositions in the range CST60-CST82 by Mitsui and Westphal (1961), Ranjan *et al* (2000), Ranjan and Pandey (2001a), Mishra *et al* (2002), (2006a) and Anwar and Lalla (2007). Apart from the shift in temperature associated with changing composition, the heating and cooling sequence in figure 1 of Anwar and Lalla (2007) for CST70 is essentially indistinguishable from the pattern for CST65 in figure 2 of the present study. The estimated transition temperatures given in a number of different studies and summarized in figure 1 also generally overlap, though the most recent dielectric data for CST70 of Anwar and Lalla (2007) seem to fall below the main trend, as does the data point for CST74 from the present study (figure 1). The dip in Young's modulus reported by Daniels *et al* (2006) for CST70 and CST80 is similar in form and magnitude to the dip in G observed in the present study for CST65. However, the former occur in the vicinity of ∼110 and ∼60 K, whereas the phase diagram in figure 1 has the $I4/mcm \leftrightarrow Pbcm$ transition placed at ∼240 and ∼120 K at these compositions. Additional elastic and anelastic anomalies observed by Daniels *et al* (2006) in CST60, CST70 and CST80 at temperatures between ∼250 and ∼270 K are different from any observed for CST65 in the present study and also do not match up with expected transition temperatures summarized in the phase diagram. Daniels *et al* proposed that the discrepancies in transition temperatures, at least, could be attributed to different sample preparation and analysis techniques.

There is general agreement that the low temperature phase for compositions in the range CST59–CST87 has $Pbcm$ symmetry (Ranjan *et al* 2000, 2001, Ranjan and Pandey 2001b, Carpenter *et al* 2006b, Daniels *et al* 2006, Mishra *et al* 2006a, 2006b, Anwar and Lalla 2008, Howard *et al* 2008). General agreement does not exist in relation to the nature of the CST structure in the temperature interval immediately above the transition interval, however. The most recent studies favour (not necessarily for exactly the same compositions) $C2/m$ or $P2_1/m$ (Woodward *et al* 2006), $Imma$ (Ranjan and Pandey

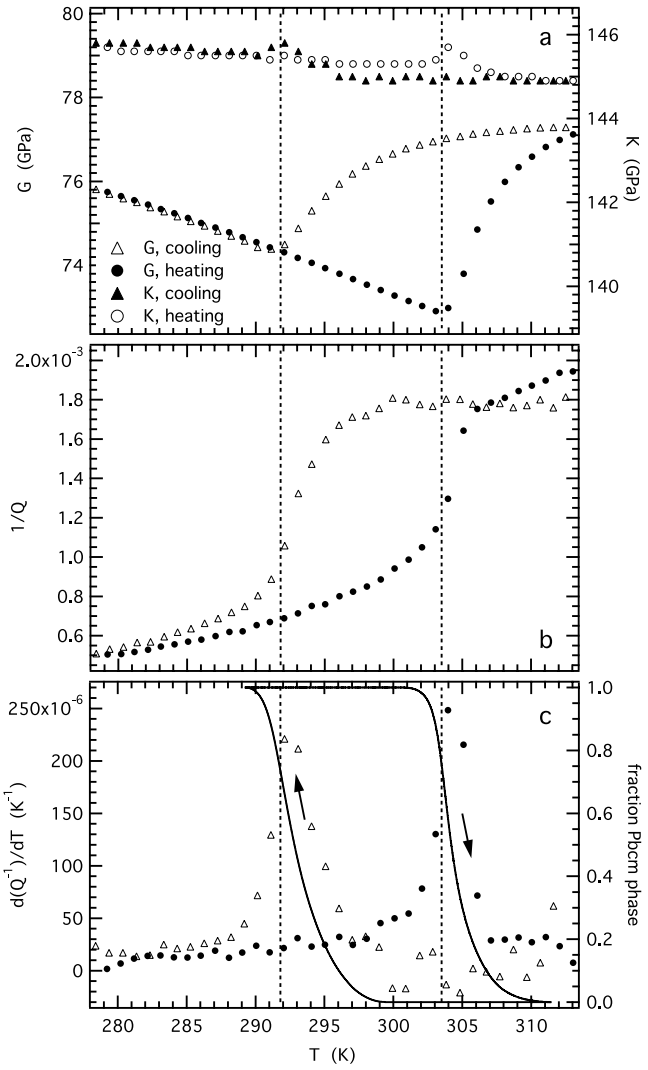

Figure 7. Elastic (a) and anelastic (b) parameters determined from the spectra shown in figure 6. Experimental uncertainties from the fitting process are estimated to be ±∼0.8 GPa for K and ±∼0.05 GPa for G. The data points in (c) were obtained by differentiation of the data for Q^{-1} in (b). The solid lines in (c) represent the fraction of $Pbcm$ phase in the two-phase field (right axis), as determined from the variation of latent heat with temperature. Note that the inflection point in Q^{-1} (maximum of $\mathrm{d}(Q^{-1})/\mathrm{d}T$) and the fraction of $Pbcm$ phase present coincide with a maximum in K and a minimum in G in both the heating and cooling sequences. The temperatures of these points are indicated by vertical lines.

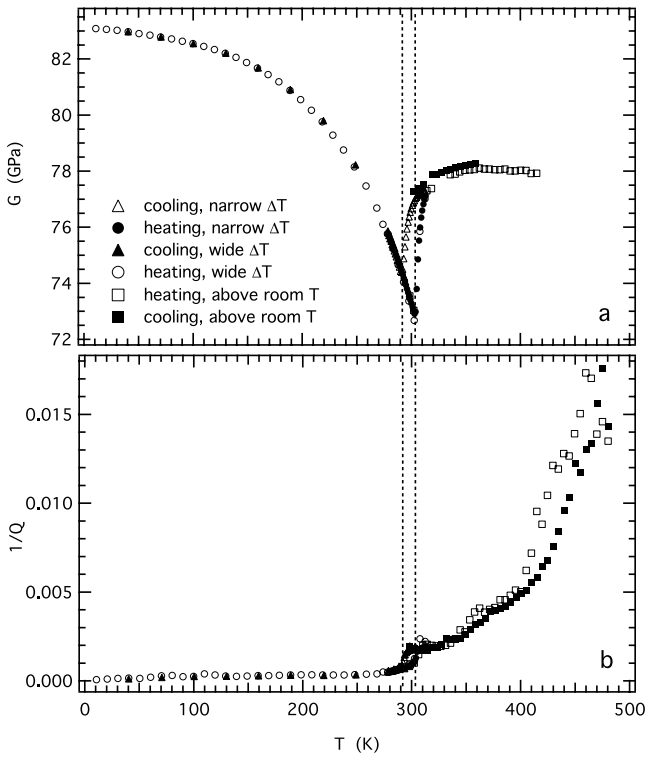

Figure 8. Variations of shear modulus, G, and acoustic dissipation parameter, Q^{-1}, over a wide temperature interval away from the $I4/mcm \leftrightarrow Pbcm$ transition interval in CST65. Dotted vertical lines have been placed at the same temperatures as those shown in figure 7.

2001b, Mishra *et al* 2002, Ranson *et al* 2005, Mishra *et al* 2005, 2006a, 2006b), $Pnma$ (Daniels *et al* 2006, Anwar and Lalla 2008), $I4/mcm$ (Qin *et al* 2000, 2002, Yamanaka *et al* 2002, Howard *et al* 2005, Carpenter *et al* 2006b, Hui *et al* 2007) or a mixture of $Pnma+P2_12_12$ (Anwar and Lalla 2007). Single crystal x-ray diffraction data of CST65, specifically, can be refined under $I4/mcm$ symmetry (Yamanaka *et al* 2002), and Carpenter *et al* (2006b) have argued that the combined data for lattice parameters and octahedral tilt angles at different compositions across the entire CST solid solution are consistent with $I4/mcm$. For the present, therefore, the transition observed in the present study is being treated as if it involves the symmetry change $I4/mcm \leftrightarrow Pbcm$.

4.1. Characteristic features of the $I4/mcm \leftrightarrow Pbcm$ transition, in comparison with $I4/mcm \leftrightarrow Pnma$

All the experimental data produced here and in previous works referred to above are consistent with the $I4/mcm \leftrightarrow Pbcm$ transition being first order in character. This is a requirement of symmetry in that the $I4/mcm$ and $Pbcm$ structures do not have a group–subgroup relationship. Exactly the same situation pertains for $I4/mcm$ and $Pnma$ structures, and there are many close similarities between the $I4/mcm \leftrightarrow Pbcm$ and $I4/mcm \leftrightarrow Pnma$ transitions. Data for CST56 and CST63 reproduced in figure 9 from Carpenter *et al* (2006b) show, in particular, that the evolution of macroscopic spontaneous strains and octahedral tilt angles are almost indistinguishable for the two transitions. In both cases, there is also a 20–30 K field of two-phase coexistence between the stability fields of the high and low symmetry phases (e.g. Ranjan *et al* 2000, Ranjan and Pandey 2001b, Mishra *et al* 2006a, Carpenter *et al* 2006b).

Contrasts between the two-phase transitions are seen in the dielectric properties—there is an anomaly associated with $I4/mcm \leftrightarrow Pbcm$ in CST60 but not with $I4/mcm \leftrightarrow Pnma$ in CST57 (see figure 1 of Mishra *et al* 2006a). The form of this anomaly is essentially the same in heating and cooling runs though the temperature at which it occurs is ∼10–15 K higher during heating than during cooling of samples with compositions between CST60 and CST74 (Anwar and Lalla 2007, Mishra *et al* 2006a; this study). There are also some

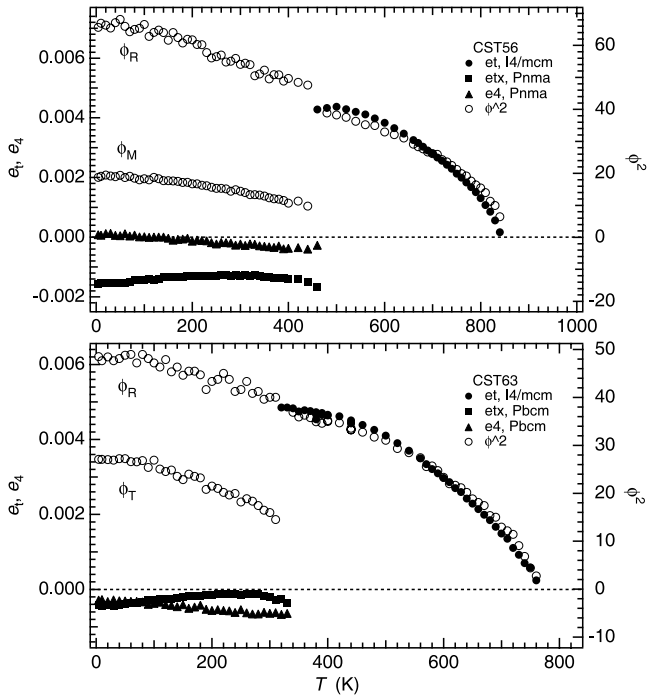

Figure 9. Variation with temperature of symmetry-adapted strains and octahedral tilt angles for CST phases which undergo the $I4/mcm \leftrightarrow Pnma$ (CST56) or the $I4/mcm \leftrightarrow Pbcm$ (CST63) transitions (reproduced from Carpenter *et al* 2006b). Small values of e_{tx} and e_4 imply that the lattice geometry of the $Pnma$ and $Pbcm$ structures is close to cubic. Subscripts R, M and T on the tilt angles refer to tilting associated with R, M and T irreps, respectively.

contrasts and similarities in the elastic properties. A change of symmetry from $I4/mcm$ to $Pnma$ is associated with an overall increase in the value of the shear modulus, as a function of composition in (Ca, Sr)TiO_3 (Carpenter *et al* 2007a, Walsh *et al* 2008) or Sr(Zr, Ti)O_3 (McKnight *et al* 2009b) and as a function of temperature in $SrZrO_3$ (McKnight *et al* 2009a). The $Pnma$ structure can be $\sim$ 20 GPa stiffer than the $I4/mcm$ structure with respect to shear. The change from $I4/mcm$ to $Pbcm$ gives an increase in the shear elastic constant but only by $\sim$4 GPa (figure 8). Variations in the bulk modulus are much smaller both for $I4/mcm \leftrightarrow Pnma$, as indicated by the composition dependence of K at room temperature in (Ca, Sr)TiO_3 and Sr(Zr, Ti)O_3 (Carpenter *et al* 2007a, Walsh *et al* 2008, McKnight *et al* 2009a, 2009b), and for $I4/mcm \leftrightarrow Pbcm$ (this study).

Finally, both the $Pnma$ and $Pbcm$ phases have very low values of Q^{-1} in comparison with $I4/mcm$ phases (Walsh *et al* 2008, McKnight *et al* 2009a, 2009b). This is consistent with the speculation of McKnight *et al* (2009b) that transformation twin walls become effectively immobile in crystals which have undergone phase transitions with two separate order parameters. However, Anwar and Lalla (2008) reported a substantial change in microstructure associated with transformation from the $Pnma$ structure to the $Pbcm$ structure. Changes in microstructure at a transition from $I4/mcm$ to $Pbcm$ could also contribute to a change in Q^{-1} but these have not yet been characterized.

4.2. Latent heat and the proportion of material transformed

The high resolution calorimetric data presented above allow details of structure–property relations in the two-phase field to be examined quantitatively for the first time. Differences in shear strain between the $I4/mcm$ and $Pbcm$ phases are less than $\sim$0.005 (figure 9) and differences in volume strain are less than 0.001 (see figure 5 of Carpenter *et al* 2006b). As a consequence, any strain energy associated with interfaces between domains with $I4/mcm$ and $Pbcm$ structure should be rather small, and the observed latent heat must arise essentially because of the difference in enthalpy of the two structures. On this basis, the latent heats extracted from the data shown in figure 4 can be used as a measure of the volume proportion transformed at any temperature within the two-phase field. Integration of the total latent heat absorbed/dissipated during heating/cooling yields curves for transformation progress as a function of temperature for CST65, which have been added to figure 7(c). Note that heating and cooling pathways are closely similar and that the point on each transformation curve where the curvature changes from concave up to concave down coincides, within experimental uncertainty, with the same point in curves for Q^{-1} and the dielectric permittivity. It is also coincident with the temperature at which G reaches a minimum and K reaches a maximum.

4.3. Structure–property behaviour of two-phase mixtures

Using the latent heat as a measure of transformation progress leads to a simple explanation of the dielectric anomaly and of the variation of Q^{-1} through the two-phase field. Figure 10(a) shows the dielectric permittivity and figure 10(b) the acoustic dissipation parameter, Q^{-1}, plotted against proportion of $Pbcm$ phase derived from the latent heat. In both cases, the data are close to being linear for heating and cooling, implying that ε' and Q^{-1} of the two-phase mixtures are merely linear combinations of the values for the pure phases according to their proportions by volume.

Shear and bulk moduli display distinctly non-linear variations as a function of the fraction transformed (figure 11(a)). There are shallow minima in G and shallow maxima in K at the temperatures where the rate of transformation with per unit of temperature change reaches a maximum (291.8 K during cooling and 303.5 K during heating). A standard treatment for calculating the bulk and shear moduli of two-phase intergrowths is that of Hashin and Shtrikman (1963), who derived expressions for upper and lower limits of the range of possible values according the elastic properties of the pure end-member phases and their proportions by volume. It is generally assumed that the elastic constants of the individual end-member phases do not change in the two-phase mixtures. This is not the case here but the Hashin–Shtrikman relations still provide a limiting case against which the behaviour across the two-phase region of a first order phase transition can be compared. Fixed values of $K = 145.0$ and 145.6 have first been assigned to the $I4/mcm$ and $Pbcm$ structures respectively. G for the $Pbcm$ structure was given a linear temperature dependence of $G = 111.63$–0.1278 T, based on a fit to data from the cooling run between 293 and 303 K. Various linear variations with temperature of

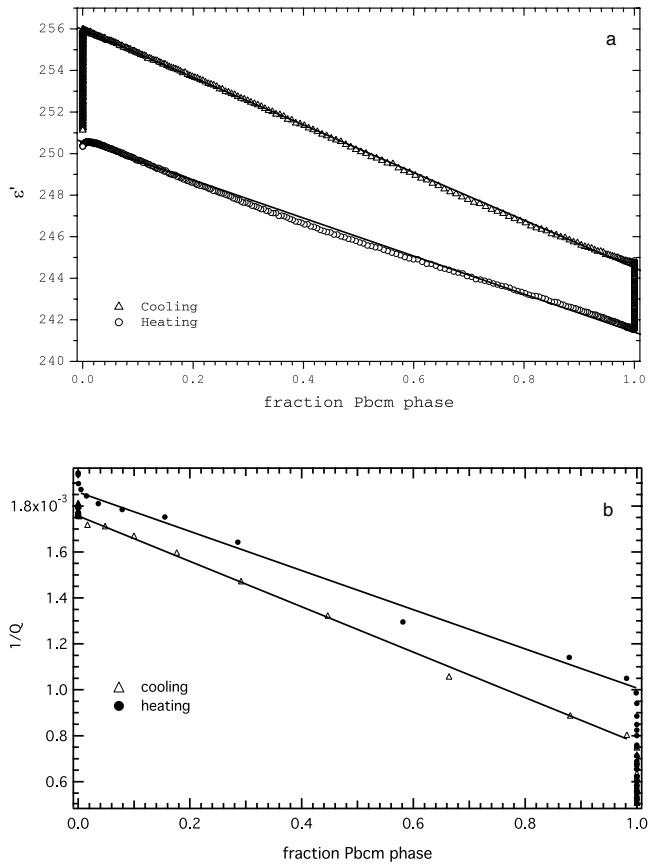

Figure 10. Linear variations of the dielectric constant, ε', and acoustic dissipation parameter, Q^{-1}, as a function of the fraction of $Pbcm$ phase present in the two-phase interval of the $I4/mcm \leftrightarrow Pbcm$ transition in CST65.

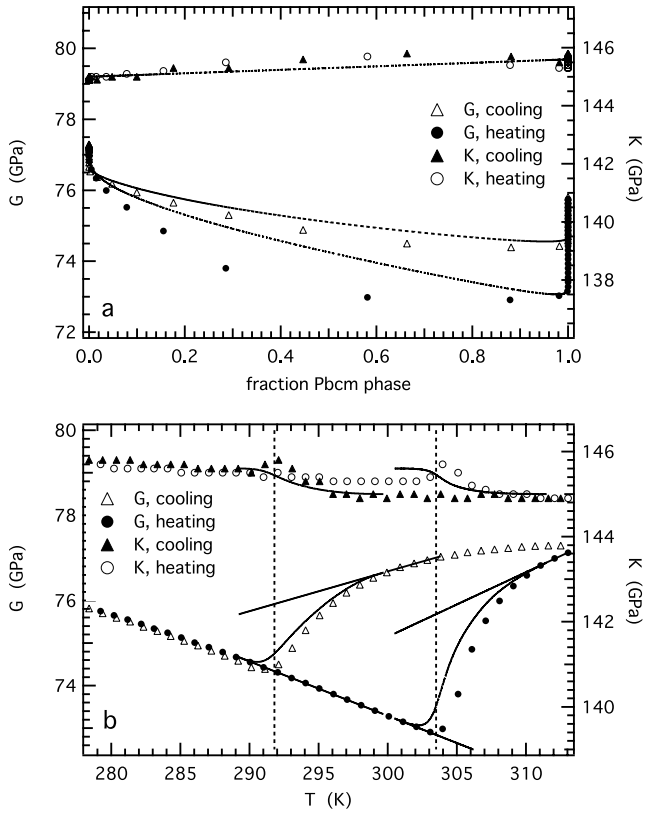

Figure 11. Observed and calculated variations of bulk modulus, K, and shear modulus, G, for CST65 as a function of volume fraction of the $Pbcm$ phase in the two-phase interval (a), and as a function of temperature (b). Dotted lines are calculated variations based on the Hashin–Shtrikman equations for the elastic properties of two-phase mixtures but, in this case, the elastic constants of the individual phases have been given linear temperature dependences, as indicated by the straight lines in (b). Upper and lower Hashin–Shtrikman bounds are indistinguishable because the elastic properties of the separate phases are similar. Calculated values of K as a function of the $Pbcm$ fraction are indistinguishable between heating and cooling.

G for the $I4/mcm$ phase were then tried in calculations of the Hashin–Shtrikman upper and lower bounds for the mixed system. Use of a fixed value of G for the $I4/mcm$ and of various linear temperature dependences based on fits to the high temperature data did not produce anything like good matches with the experimental data. Calculated variations for the mixed phases shown as a function volume proportion in figure 11(a) and as a function of temperature in figure 11(b) represent the case of linear behaviour of G for $I4/mcm$ at the high temperature limit of the transition interval. These give the correct pattern of variation but do not produce a quantitative match. Note that because the values of the elastic constants of the two end-members are not very different, the Hashin–Shtrikman upper and lower bounds are indistinguishable.

Elastic behaviour across the two-phase interval for $I4/mcm \leftrightarrow Pbcm$ clearly depends on variations of the elastic properties of the $I4/mcm$ and $Pbcm$ phases in the vicinity of and through the transition interval. When the two phases are intimately intergrown, strains at the interfaces between them may well influence the strain within each and, hence, the amount of renormalization of their elastic constants by strain/order parameter coupling. If the interfaces become important in determining the bulk elastic properties, it is necessary to consider contributions to the Hashin–Shtrikman equations which are second order in the volume fractions (Salje 2007). Clearly the expectation must be that the topology of the intergrowths will be important and, in this context, Anwar and Lalla (2008) found that domains of $Pbcm$ and $Pnma$ phases can coexist within single crystals rather than occurring as crystals of one phase coexisting with crystals of the second separated by grain boundaries. It follows, conversely, that details of the elastic behaviour (particularly the maxima in K and minima in G at the inflection point of the variation of volume transformed) must contain information about transformation mechanism and microstructure. There is no reason to suppose that the transition in CST65 is in any way unique and it is likely that the same structure/microstructure–property relations will apply at other first order transitions in perovskites.

4.4. Symmetry aspects of the $I4/mcm$–$Pbcm$ transition

Octahedral tilting in the $I4/mcm$ structure is associated with the R point of the Brillouin zone of the parent cubic ($Pm\bar{3}m$) structure; the relevant irrep is R_4^+. The $Pnma$ structure contains $Imma$ tilting from the R point plus a second tilt

system associated with the M point, for which the irrep is M_3^+. As discussed in Carpenter *et al* (2006b) and Howard *et al* (2008), structural changes which accompany the transition to $Pbcm$ symmetry can be understood in terms, firstly of a change from the $I4/mcm$ to the $Imma$ tilt system of R_4^+, and secondly of antiferroelectric displacements associated with the $\xi = 1/4$ point on the Δ line of symmetry ($\mathbf{k} = [1/2, 1/2, \xi]^*$) plus octahedral tilting associated with the $\xi = 1/4$ point on the T line of symmetry between the R and M points ($\mathbf{k} = [1/2, 1/2, \xi]^*$). The Δ and T irreps are Δ_5 and T_4 (Howard *et al* 2008; see also Mishra *et al* 2006b). Normal mode analysis of refined atomic coordinates for CST63 suggests that the T_4 octahedral tilting is predominant, but with small Δ_5 antiferroelectric displacements of Ca/Sr and Ti (Howard *et al* 2008). The T_4 tilting involved can be thought of as being only one particular tilt mode out of a range of possibilities along the R–M line. In this context, it is interesting to note that Howard *et al* (2008) observed streaking along the whole line in electron diffraction patterns, which could imply that all these tilt modes are low-lying in energy terms. That any energetic differences between the T_4 and M_3^+ tilt systems are small is implied also by the similarities in tilt angle and strain evolution for $I4/mcm \leftrightarrow Pnma$ and $I4/mcm \leftrightarrow Pbcm$ transitions shown in figure 9. If the energies of the second tilt systems, T_4 and M_3^+ are indeed the same, the additional antiferroelectric displacement could be sufficient to stabilize the $Pbcm$ structure ahead of the $Pnma$ structure, even if the displacements are only small.

A measure of the antiferroelectric contribution to the stability of the $Pbcm$ structure is provided by the magnitude of the change in ε' of the $I4/mcm$ and $Pbcm$ phases, which from the interpretation provided above is simply the difference in values of the two phases at the transition point, $\Delta\varepsilon'$ (figure 2). Figure 1 of Ranjan *et al* (2000) shows that this step is largest at Sr-rich compositions (e.g. CST77), that it diminishes with increasing Ca-content and that it would extrapolate to zero close to CST60. From the phase diagram, ~CST59 is the composition at which the $Pbcm$ and $Pnma$ structures have the same energy, while increasing Sr-content causes the $I4/mcm \leftrightarrow Pbcm$ transition to be displaced to progressively higher temperatures above the extrapolation of the $I4/mcm \leftrightarrow Pnma$ transition. In other words, the correlation of increasing difference in transition temperature correlates with increasing $\Delta\varepsilon'$ is consistent with the view that the $Pbcm$ tilt system is stabilized by the antiferroelectric displacement by an amount that increases with increasing Sr-content. It is not clear whether weak coupling of the tilts and antiferroelectric displacements with shear strains and volume strain is an additional requirement favouring this change of the energy balance, but the orthorhombic structures have lattice geometry which is close to being cubic in this composition range (Mitsui and Westphal 1961, Ball *et al* 1998, Ranjan and Pandey 1999, 2001b, Ranjan *et al* 1999, 2001, Carpenter *et al* 2001, 2006b, Mishra *et al* 2002, 2006a, 2006b).

The total excess entropy measured for the $I4/mcm \leftrightarrow Pbcm$ transition would remain well below an estimate of configurational entropy given by $-R \ln 2 = -5.8\ \mathrm{J\ mol^{-1}\ K^{-1}}$ for a two component order–disorder system even if a linear extrapolation of the variation of ΔS shown in figure 5 was applied down to 0 K. This indicates that both the tilting and antiferroelectric displacements of the $Pbcm$ structure are probably displacive rather than order–disorder in origin.

4.5. Precursor softening on either side of the transition

The observed pattern of precursor softening for the $I4/mcm \leftrightarrow Pbcm$ transition is not unique. For example, distinct and non-linear reductions in the shear modulus of $SrZrO_3$ occur as a function of temperature when the $I4/mcm \leftrightarrow Imma$ octahedral tilting transition is approached from either side (McKnight *et al* 2009a, 2009b) and the same behaviour appears to extend across Sr(Zr, Ti)O_3 solid solution (McKnight *et al* 2009b). A similar pattern of softening is found at the cooperative Jahn–Teller ordering transition in $La_{1-x}Ca_xMnO_3$ (Zheng *et al* 2002) and at the first order $P4mm \leftrightarrow Amm2 \leftrightarrow R3m$ transitions in $BaTiO_3$ (Cheng *et al* 1994, Zhang *et al* 1994), which involve changes in the orientation of ferroelectric displacements. In the present case, the softening extends to at least ~50 K away from the transition itself and the detailed latent heat data reveal that this is well outside the interval of two-phase coexistence. Furthermore, the lack of a peak in the dissipation, Q^{-1}, through the transition interval implies that movement of interfaces between coexisting $I4/mcm$ and $Pbcm$ phases is not a factor. The behaviour appears to be intrinsic, therefore, and the most obvious possible mechanisms are clustering/fluctuations and optic mode softening (with coupling to acoustic modes). Experimental methods which probe the local phonon scale dynamics, such as optical spectroscopy, would be needed to discriminate between these. If there is a signal in the heat capacity associated with such dynamical behaviour, the data suggest that it is only very small.

In contrast with the elastic softening, the pattern of changes in Q^{-1} at the $I4/mcm \leftrightarrow Pbcm$ transition is quite different from that observed in $La_{1-x}Ca_xMnO_3$ (Zheng *et al* 2002) or $BaTiO_3$ (Cheng *et al* 1994, Zhang *et al* 1994) in not showing a distinct peak centred on the transition point. As already implied in the discussion above, this is being interpreted here as indicating that any interfaces between $I4/mcm$ and $Pbcm$ domains do not move on the timescale of applied stresses in the RUS measurements (~10^{-6} s). The strong temperature dependence of Q^{-1} in the stability field of the $I4/mcm$ structure is being interpreted, by analogy with similar temperature dependence for low frequency acoustic dissipation in CST perovskites by Harrison *et al* (2003), in terms of transformation twin wall movements. There remains the possibility that clustering or phonon softening could also give rise to an intrinsic acoustic damping, however.

5. Conclusions

Detailed measurements of dielectric permittivity, latent heat, elastic constants and acoustic dissipation from a single polycrystalline sample of $Ca_{0.35}Sr_{0.65}TiO_3$ perovskite have allowed precise correlations between these properties to be followed during heating and cooling through the first order $I4/mcm \leftrightarrow Pbcm$ transition. Changes in the dielectric

constant and in acoustic dissipation can be understood simply in terms of linear combinations of the properties of the separate phases according to their volume proportions across a two-phase interval which is ∼11 K wide. The elastic constants are not additive in the same way but are consistent with the elastic behaviour of two-phase intergrowths more generally if K and G of the $I4/mcm$ and $Pbcm$ structures continue to have a significant temperature dependence within the two-phase field. The total latent heat for the transition diminishes with increasing $SrTiO_3$ content and this correlates with an increasing importance of antiferroelectric displacements in the $Pbcm$ structure, as deduced from data in the literature for the dielectric anomaly. It is not clear that the lack of measured latent heat at $Ca_{0.26}Sr_{0.74}TiO_3$ implies that the transition could become continuous, however. There appear to be close parallels between the $I4/mcm \leftrightarrow Pnma$ and $I4/mcm \leftrightarrow Pbcm$ transitions in the (Ca, Sr)TiO_3 system and it is expected that the evolution of elastic and calorimetric properties might be typical, more generally, of first order transitions in perovskites where there is no group–subgroup relationship between the high and low symmetry phases. The primary difference between the $Pnma$ and $Pbcm$ structures seems to be in the second tilt system according to whether there is the additional possibility of coupling with atomic displacements which give rise to electric dipoles. In the $Pnma$ structure the energetically favoured second tilt system is associated with irrep M_3^+ and in the $Pbcm$ structure it is associated with irrep T_4. The latter is preferred in $SrTiO_3$-rich compositions by coupling with antiferroelectric displacement scheme associated with irrep Δ_5, and is a reflection of the well-known tendency for relaxor or ferroelectric type atomic displacements to develop at low temperatures in $SrTiO_3$ doped with Ca. From the small entropy changes involved, these changes are probably all displacive rather than order–disorder in origin.

Acknowledgments

We thank A I Becerro for supplying CST68 and CST74 samples. The calorimetric and dielectric experiments have been supported in Seville by Project FIS2006-04045. J Manchado wishes to thank Fundación Cámara for a research grant. The RUS equipment in Cambridge was purchased with a grant from the Natural Environment Research Council (NER/A/S2000/01055).

References

Anwar S and Lalla N P 2007 Space group analysis of $Sr_{1-x}Ca_xTiO_3$ ceramics with $x = 0.20$, 0.27 and 0.30 through electron diffraction *J. Phys.: Condens. Matter* **19** 436210

Anwar S and Lalla N P 2008 Electron microscope studies of the antiferroelectric phase in $Sr_{0.60}Ca_{0.40}TiO_3$ ceramic *J. Solid State Chem.* **181** 997–1004

Ball C J, Begg B D, Cookson D J, Thorogood G J and Vance E R 1998 Structures in the system $CaTiO_3/SrTiO_3$ *J. Solid State Chem.* **139** 238–47

Bednorz J G and Müller K A 1984 $Sr_{1-x}Ca_xTiO_3$: an XY quantum ferroelectric with transition to randomness *Phys. Rev. Lett.* **52** 2289–92

Bianchi U 1996 *PhD Thesis* Gerhard-Marcator Universität, Duisburg

Bianchi U, Dec J, Kleemann W and Bednorz J G 1995 Cluster and domain-state dynamics of ferroelectric $Sr_{1-x}Ca_xTiO_3$ ($x = 0.007$) *Phys. Rev.* B **51** 8737–46

Bianchi U, Kleemann W and Bednorz J G 1994a Ferroelectric domain state transition of $SrTiO_3$:Ca *Ferroelectrics* **157** 165–70

Bianchi U, Kleemann W and Bednorz J G 1994b Raman scattering of ferroelectric $Sr_{1-x}Ca_xTiO_3$, $x = 0.007$ *J. Phys.: Condens. Matter* **6** 1229–38

Carpenter M A 2007a Elastic anomalies accompanying phase transitions in (Ca, Sr)TiO_3 perovskites: part I. Landau theory and a calibration for $SrTiO_3$ *Am. Mineral.* **92** 309–27

Carpenter M A 2007b Elastic anomalies accompanying phase transitions in (Ca, Sr)TiO_3 perovskites: part II. Calibration for the effects of composition and pressure *Am. Mineral.* **92** 328–43

Carpenter M A, Becerro A I and Seifert F 2001 Strain analysis of phase transitions in (Ca, Sr)TiO_3 perovskites *Am. Mineral.* **86** 348–63

Carpenter M A, Darling T W, Bass J D, Lakshtanov D L, Sinogeikin S V and Jacobsen S D 2006a Superattenuation of acoustic resonances and non-linear elasticity associated with the cubic–rhombohedral phase transition in $LaAlO_3$ perovskite *Eos Trans. AGU* **87** Fall Meet. Suppl. Abstract MR3A01

Carpenter M A, Howard C J, Knight K S and Zhang Z 2006b Structural relationships and a phase diagram for (Ca, Sr)TiO_3 perovskites *J. Phys.: Condens. Matter* **18** 10725–49

Carpenter M A, Li B and Liebermann R C 2007a Elastic anomalies accompanying phase transitions in (Ca, Sr)TiO_3 perovskites: part III. Experimental investigation of polycrystalline samples *Am. Mineral.* **92** 344–55

Carpenter M A, Rios S, Sondergeld P, Crichton W and Bouvier P 2007b Structural evolution of $(Ca_{0.35}Sr_{0.65})TiO_3$ at high pressures *J. Solid State Chem.* **180** 360–9

Cheng B L, Gabbay M, Fantozzi G and Duffy W Jr 1994 Mechanical loss and elastic modulus associated with phase transitions of barium titanate ceramics *J. Alloys Compounds* **211/212** 352–5

Daniels J E, Elcombe M M, Finlayson T R and Vance E R 2006 Neutron diffraction study of polycrystalline $Ca_{1-x}Sr_xTiO_3$ mixed perovskite materials *Physica* B **385/386** 88–90

del Cerro J 1988 Simultaneous measurement of thermal properties in ferroelectric crystals *J. Therm. Anal.* **34** 335–44

del Cerro J, Martín-Olalla J M and Romero F J 2003 Square modulated differential thermal analysis *Thermochim. Acta* **401** 149–58

del Cerro J, Romero F J, Gallardo M C, Hayward S A and Jiménez J 2000 Latent heat measurement near a tricritical point: a study of the $KMnF_3$ ferroelastic crystal *Thermochim. Acta* **343** 89–97

Delgado-Sánchez J M, Martín-Olalla J M, Gallardo M C, Ramos S, Koralewski M and del Cerro J 2005 The influence of an electric field on the latent heat of the ferroelectric phase transition in KDP *J. Phys.: Condens. Matter* **17** 2645–54

Gallardo M C, Becerro A I, Romero F J, del Cerro J, Seifert F and Redfern S A T 2003 Cubic–tetragonal phase transition in $Ca_{0.04}Sr_{0.96}TiO_3$: a combined specific heat and neutron diffraction study *J. Phys.: Condens. Matter* **15** 91–100

Gallardo M C, Jiménez J and del Cerro J 1995 Experimental device for measuring the influence of a uniaxial-stress on specific heat. Application to the strontium titanate ferroelastic crystal *Rev. Sci. Instrum.* **66** 5288–91

Gallardo M C, Romero F, Hayward S, Salje E and del Cerro J 2000 Phase transitions in perovskites near the tricritical point: an experimental study: an experimental study of $KMn_{1-x}Ca_xF_3$ and $SrTiO_3$ *Mineral. Mag.* **64** 971–82

Guyot F, Richet P, Courtial P and Gillet P 1993 High-temperature heat-capactity and phase-transitions of $CaTiO_3$ perovskite *Phys. Chem. Miner.* **20** 141–6

Harrison R J, Redfern S A T and Street J 2003 The effect of transformation twins on the seismic-frequency mechanical properties of polycrystalline $Ca_{1-x}Sr_xTiO_3$ perovskite *Am. Mineral.* **88** 574–82

Hashin Z and Shtrikman S 1963 A variational approach to the theory of the elastic behaviour of multiphase materials *J. Mech. Phys. Solids* **11** 127–40

Hayward S A and Salje E K H 1999 Cubic-tetragonal phase transition in $SrTiO_3$ revisited: Landau theory and transition mechanism *Phase Transit.* **68** 501–22

Hirata T, Ishioka K and Kitajima M 1996 Vibrational spectroscopy and x-ray diffraction of perovskite compounds $Sr_{1-x}M_xTiO_3$ (M = Ca, Mg; $0 \leqslant x \leqslant 1$) *J. Solid State Chem.* **124** 353–9

Howard C J, Withers R L and Kennedy B J 2001 Space group and structure for the perovskite $Ca_{0.5}Sr_{0.5}TiO_3$ *J. Solid State Chem.* **160** 8–12

Howard C J, Withers R L, Knight K S and Zhang Z 2008 $(Ca_{0.37}Sr_{0.63})TiO_3$ perovskite—an example of an unusual class of tilted perovskites *J. Phys.: Condens. Matter* **20** 135202

Howard C J, Withers R L, Zhang Z, Osaka K, Kato K and Takata M 2005 Space-group symmetry for the perovskite $Ca_{0.3}Sr_{0.7}TiO_3$ *J. Phys.: Condens. Matter* **17** L459–65

Hui Q, Dove M T, Tucker M G, Redfern S A T and Keen D A 2007 Neutron total scattering and reverse Monte Carlo study of cation ordering in $Ca_xSr_{1-x}TiO_3$ *J. Phys.: Condens. Matter* **19** 335214

Jiménez J, Rojas E and Zamora M 1984 Design and construction of precision heat fluxmeters *J. Appl. Phys.* **56** 3353–6

Kleemann W, Albertini A, Kuss M and Lindner R 1997 Optical detection of symmetry breaking on a nanoscale in $SrTiO_3$:Ca *Ferroelectrics* **203** 57–64

Kleemann W, Bianchi U, Bürgel A, Prasse M and Dec J 1995 Domain state properties of weakly doped $SrTiO_3$:Ca *Phase Transit.* **55** 57–68

Ledbetter H, Lei M, Hermann A and Sheng Z 1994 Low-temperature elastic constants of $Y_1Ba_2Cu_3O_7$ *Physica* C **225** 397–403

Lemanov V V 1997 Phase transitions in $SrTiO_3$-based solid solutions *Phys. Solid State* **39** 1468–73

Martín-Olalla J M, del Cerro J and Ramos S 2000 Evidence of latent heat in the Rb_2ZnCl_4 commensurate-incommensurate phase transition *J. Phys.: Condens. Matter* **12** 1715–22

McKnight R E A, Carpenter M A, Darling T W, Buckley A and Taylor P A 2007 Acoustic dissipation associated with phase transitions in lawsonite, $CaAl_2Si_2O_7(OH)_2{\cdot}H_2O$ *Am. Mineral.* **92** 1665–72

McKnight R E A, Howard C J and Carpenter M A 2009a Elastic anomalies associated with transformation sequences in perovskites: I. Strontium zirconate, $SrZrO_3$ *J. Phys.: Condens. Matter* **21** 015901

McKnight R E A, Kennedy B J, Zhou Q and Carpenter M A 2009b Elastic anomalies associated with transformation sequences in perovskites: II. The strontium zirconate-titanate Sr(Zr, Ti)O_3 series *J. Phys.: Condens. Matter* **21** 015902

McKnight R E A, Moxon T, Buckley A, Taylor P A, Darling T W and Carpener M A 2008 Grain size dependence of elastic anomalies accompanying the α–β phase transition in polycrystalline quartz *J. Phys.: Condens. Matter* **20** 075229

Migliori A and Sarrao J L 1997 *Resonant Ultrasound Spectroscopy: Applications to Physics, Materials Measurements and Nondestructive Evaluation* (New York: Wiley)

Mishra S K, Ranjan R, Pandey D and Kennedy B J 2002 Powder neutron diffraction study of the antiferroelectric phase transition in $Sr_{0.75}Ca_{0.25}TiO_3$ *J. Appl. Phys.* **91** 4447–52

Mishra S K, Ranjan R, Pandey D, Ouillon R, Pinan-Lucarre J-P, Ranson P and Pruzan Ph 2001 A Raman scattering study of the antiferrroelectric phase transition in $(Sr_{0.70}Ca_{0.30})TiO_3$ *Phys. Rev.* **64** 092302

Mishra S K, Ranjan R, Pandey D, Ranson P, Ouillon R, Pinan-Lucarre J-P and Pruzan Ph 2005 A combined x-ray diffraction and Raman scattering study of the phase transitions in $Sr_{1-x}Ca_xTiO_3$ ($x = 0.04, 0.06, 0.12$) *J. Solid State Chem.* **178** 2846–57

Mishra S K, Ranjan R, Pandey D, Ranson P, Ouillon R, Pinan-Lucarre J-P and Pruzan Ph 2006a Resolving the controversies about the 'nearly cubic' and other phases of $Sr_{1-x}Ca_xTiO_3$ ($0 \leqslant x \leqslant 1$): II. Comparison of phase transition behaviours for $x = 0.40$ and 0.43 *J. Phys.: Condens. Matter* **18** 1899–912

Mishra S K, Ranjan R, Pandey D and Stokes H T 2006b Resolving the controversies about the 'nearly cubic' and other phases of $Sr_{1-x}Ca_xTiO_3$ ($0 \leqslant x \leqslant 1$): I. Room temperature structures *J. Phys.: Condens. Matter* **18** 1885–98

Mitsui T and Westphal W B 1961 Dielectric and x-ray studies of $Ca_xBa_{1-x}TiO_3$ and $Ca_xSr_{1-x}TiO_3$ *Phys. Rev.* **124** 1354–9

Ouillon R, Pinan-Lucarre J-P, Ranson P, Pruzan Ph, Mishra S K, Ranjan R and Pandey D 2002 A Raman scattering study of the phase transitions in $SrTiO_3$ and in the mixed system $(Sr_{1-x}Ca_x)TiO_3$ at ambient pressure from $T = 300$ down to 8 K *J. Phys.: Condens. Matter* **14** 2079–92

Qin S, Becerro A I, Seifert F, Gottsmann J and Jiang J 2000 Phase transitions in $Ca_{1-x}Sr_xTiO_3$ perovskites: effects of composition and temperature *J. Mater. Chem.* **10** 1609–15

Qin S, Wu X, Seifert F and Becerro A I 2002 Micro-Raman study of perovskites in the $CaTiO_3$–$SrTiO_3$ system *J. Chem. Soc., Dalton Trans.* **2002** 3751–5

Ranjan R and Pandey D 1999 Novel structural features and phase transition behaviour of $(Sr_{1-x}Ca_x)TiO_3$: II. X-ray diffraction studies *J. Phys.: Condens. Matter* **11** 2247–58

Ranjan R and Pandey D 2001a Antiferroelectric phase transition in $(Sr_{1-x}Ca_x)TiO_3$ ($0.12 \leqslant x \leqslant 0.40$): I. Dielectric studies *J. Phys.: Condens. Matter* **13** 4239–49

Ranjan R and Pandey D 2001b Antiferroelectric phase transition in $(Sr_{1-x}Ca_x)TiO_3$: II. X-ray diffraction studies *J. Phys.: Condens. Matter* **13** 4251–66

Ranjan R, Pandey D and Lalla N P 2000 Novel features of $Sr_{1-x}Ca_xTiO_3$ phase diagram: evidence for competing antiferroelectric and ferroelectric interactions *Phys. Rev. Lett.* **84** 3726–9

Ranjan R, Pandey D, Schuddinck W, Richard O, De Meulenaere P, Van Landuyt J and Van Tendeloo G 2001 Evolution of crystallographic phases in $(Sr_{1-x}Ca_x)TiO_3$ with composition (x) *J. Solid State Chem.* **162** 20–8

Ranjan R, Pandey D, Siruguri V, Krishna P S R and Paranjpe S K 1999 Novel structural features and phase transition behaviour of $(Sr_{1-x}Ca_x)TiO_3$: I. Neutron diffraction study *J. Phys.: Condens. Matter* **11** 2233–46

Ranson P, Ouillon R, Pinan-Lucarre J-P, Pruzan Ph, Mishra S K, Ranjan R and Pandey D 2005 The various phases of the system $Sr_{1-x}Ca_xTiO_3$—a Raman scattering study *J. Raman Spectrosc.* **36** 898–911

Ringwood A E, Kessom S E, Reeve K D, Levins D M and Ramm E J 1988 *Synroc Radioactive Waste Forms for the Future* ed W Lutze and R C Ewing (Amsterdam: North Holland) pp 233–4

Romero F J, Gallardo M C, Czarnecka A, Koralewski M and del Cerro J 2007 Thermal and kinetic study of the ferroelectric phase transition in deuterated triglycine selenate *J. Therm. Anal. Cal.* **87** 355–61

Romero F J, Gallardo M C and del Cerro J 2006 Phase coexistence in highly deuterated ferroelectric triglycine selenate: Landau description *Europhys. Lett.* **76** 863–9

Romero F J, Gallardo M C, Jiménez J, Czarnecka A, Koralewski M and del Cerro J 2004a Evidence of Landau tricritical behaviour in TGSe by calorimetric measurements: effect of a weak uniaxial stress *J. Phys.: Condens. Matter* **16** 7637–48

Romero F J, Gallardo M C, Jiménez J and del Cerro J 2001 Discrimination of the transition order extremely close to the tricritical point *Thermochim. Acta* **372** 25–31

Romero F J, Jiménez J and del Cerro J 2004b Calorimetric investigation on the paramagnetic–antiferromagnetic phase transition in CoO *J. Magn. Magn. Mater.* **280** 257–63

Salje E K H 2007 An empirical scaling model for averaging elastic properties including interfacial effects *Am. Mineral.* **92** 429–32

Walsh J N, Taylor P A, Buckley A, Darling T W, Schreuer J and Carpenter M A 2008 Elastic and anelastic anomalies in

(Ca, Sr)TiO_3 perovskites: analogue behaviour for silicate perovskites *Phys. Earth Planet. Inter.* **167** 110–7

Wang C, Aguado F and Redfern S A T 2007 Discontinuous temperature-dependent macroscopic strain due to ferroelastic domain switching and structural phase transitions in barium strontium titanate *Appl. Phys. Lett.* **91** 192908

Woodward D I, Wise P L, Lee W E and Reaney I M 2006 Space group symmetry of $(Ca_xSr_{1-x})TiO_3$ determined using electron diffraction *J. Phys.: Condens. Matter* **18** 2401–8

Yamanaka T, Hirai N and Komatsu Y 2002 Structure change of $Ca_{1-x}Sr_xTiO_3$ perovskite with composition and pressure *Am. Mineral.* **87** 1183–9

Zhang J X, Zheng A, Fung P C W and Liang K F 1994 Internal friction study of transformation dynamics in $BaTiO_3$ ceramics *J. Alloys Compounds* **211/212** 378–80

Zheng R K, Huang R X, Tang A N, Li G, Li X G, Wei J N, Shui J P and Yao Z 2002 Internal friction and Jahn–Teller effect in the charge-ordered $La_{1-x}Ca_xMnO_3$ ($0.5 \leqslant x \leqslant 0.87$) *Appl. Phys. Lett.* **81** 3834–6